Some experimental studies on the sea wave dissipation over different seabeds

Sara Corvaro[1], Carlo Lorenzoni[1], Matteo Postacchini[1], Elisa Seta[1], Luciano Soldini[1], Maurizio Brocchini[1], Alessandro Mancinelli[1]

[1]*Dipartimento di Idraulica, Strade, Ambiente e Chimica (D.I.S.A.C.), Università Politecnica delle Marche, Italia*
E-mail: s.corvaro@univpm.it, c.lorenzoni@univpm.it, m.postacchini@univpm.it, e.seta@univpm.it, l.soldini@univpm.it, m.brocchini@univpm.it, a.mancinelli@univpm.it

Keywords: coastal protection, submerged structures, macro-roughness, permeability, porous bed.

SUMMARY. Some laboratory campaigns were carried out with the aim to analyze the functioning of two innovative coastal defense methods which rely on dissipative mechanisms acting either at the seabed (induced by the seabed roughness) or within the seabed itself (due to the seabed porosity) and traditional breakwaters. During the first group of tests some submerged breakwater configurations were arranged on a movable bed. In the second campaign the waves were forced to pass over vertical or inclined metal blades, lying on the bottom of the flume and covering one half of the water depth. Finally, wave dissipation was induced by a porous bed made of thousands of identical spheres, having a diameter of 36mm. The aim was to try to understand the hydrodynamics together with the kinematics induced by such configurations. Wave height decay patterns were analyzed to evaluate the efficiency of the various methods. Similar efficiencies in reducing the intensity of the incident waves were observed.

1 INTRODUCTION

The energy of sea waves is mostly dissipated (especially for mildly sloping beaches) in the surf zone, a region of the coast where breaking waves transfer much of their energy and momentum to both turbulence and currents. The narrow region over which waves break is, together with the swash zone, the region where most of the sediment transport occurs.

If the global littoral morphodynamic equilibrium, mainly governed by the wave field and by the sediment input provided by river contributions, is perturbed by anthropic factors, e.g. port constructions or river weirs, littoral erosion may occur. Coastline parallel defense structures, i.e. detached barriers (either emerged or submerged), aim to reduce the energy by making the waves break on the structures themselves. This, in turn, leads to both a large decay of the incident waves and a reduced sediment transport potential, hence contributing to stabilize the local coastal morphology.

If wave breaking is induced by submerged breakwaters a complex flow circulation is established in which the water superelevation, induced by breaking waves inshore of the breakwaters, forces, together with the large-scale horizontal eddies evolving from the breakwater heads, strong rip currents through the gaps located between contiguous breakwaters. Such currents are dangerous for both beach stability and swimmer safety.

The search of coastal defense solutions, alternative to the traditional detached breakwaters,

suggests to test new structures able to dissipate the wave energy by means of either bottom friction or permeability, so that troubles due to the violent breaking on the breakwaters can be avoided.

This paper compares the experimental results on wave height decay as induced by submerged breakwaters, macroroughness structures and permeable seabeds. The experiments were carried out at the Hydraulic Laboratory of the I.S.A.C. Department of the Università Politecnica delle Marche (Ancona).

1.1 *Wave decay on natural seabeds*

During wave propagation the energy of the waves is dissipated by various mechanisms. This can be quantified as follows:

$$\frac{\partial(EC_g)}{\partial x} = -\varepsilon_b - \varepsilon_f - \varepsilon_p \tag{1}$$

where E is the wave energy and C_g the group velocity, so that (EC_g) represents the wave energy flux; on the other hand the ε-terms are the dissipative contributions due to wave breaking (ε_b), bottom friction (ε_f) and porosity (ε_p). In the surf zone the dissipation due to breaking dominates, so that in shallow water conditions ($h/L<1/20$, L being the wavelength) it can be quantified by a bore-type breaking (see also [1]):

$$\varepsilon_b = \frac{\rho g c_{bore}}{L} h \frac{(d_2 - d_1)^3}{4 d_1 d_2} \tag{2}$$

where ρ is the water density, g the gravity acceleration, h the local undisturbed water depth, d_1 and d_2 the water levels characterizing the bore and c_{bore} the bore phase speed:

$$c_{bore} = \sqrt{\frac{g d_1 d_2 (d_1 + d_2)}{2h^2}} \tag{2a}$$

The dissipation over a rough bottom at a wave-averaged level is computed as follows:

$$\varepsilon_f = \langle \tau_b \cdot u_b \rangle = \left\langle \frac{1}{2} f \rho u_b^2 |u_b| \right\rangle \tag{3}$$

where $\langle\ \rangle$ is the time averaging operator, τ_b is the bottom shear stress, u_b the bottom velocity and f the bottom friction factor. In a recent study [2], the particular situation of vegetation growing on the seabed was studied. In this case the friction equation (3) changes into:

$$\varepsilon_f = \varepsilon_v = \frac{2}{3\pi} \rho C_D b_v N \left(\frac{kg}{2\sigma} \right)^3 \frac{\sinh(k\alpha h) + 3\sinh(k\alpha h)}{3k \cosh^3(kh)} H^3 \tag{3a}$$

where ε_v is used to indicate the vegetation-induced dissipation, k is the wavenumber, σ the wave frequency and H the wave height; then C_D is the drag coefficient, b_v, N and α some vegetation

parameters.

It is more difficult to quantify the wave energy dissipation due to the seabed porosity. However it is clear that ε_p is function of two resistance forces. The former is the inertia force f_I, which depends on the porosity (n), on the virtual mass coefficient (γ_p) and on the flow velocity (u). The latter is the drag force f_D, depending on the drag coefficient, on the porosity and on a characteristic velocity (u_c).

1.2 *Wave decay in regions protected by submerged structures*

Submerged bars or breakwaters are efficient in dissipating the energy of the incoming waves because they induce an intense wave breaking (roughness and porosity effects only providing minor contributions to the dissipation). Such a wave breaking is well described in [3], where three breaking modalities (illustrated in Figure 1) are carefully analyzed:

a. breaking only on the barrier crest (crest depth: h_c, final wave height: $H=\beta h_c$);
b. breaking only on the slope (according to the depth-limited criterion: $H=\gamma h$, where $h \leq h_b$ and h_b gives the depth at which breaking first occurs);
c. breaking on the slope (according to the depth-limited criterion) and on the barrier crest.

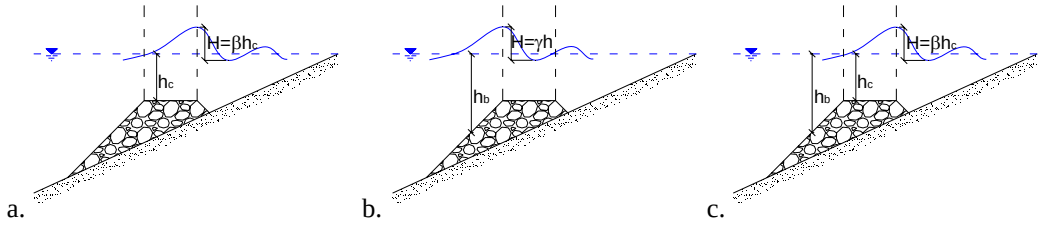

Figure 1: Sketch of three types of wave breaking in the presence of a barrier.

Typically waves start breaking on the seaward slope of the breakwater and keep breaking on the freeboard, thus, breaking-type c. is, probably, the most realistic and includes the mechanisms typical of modalities a. and b. Hence, the dissipation can be expressed by means of an equation similar to (2).

2 EXPERIMENTAL TESTS ON BEACHES PROTECTED BY SUBMERGED BARRIERS

The experimental tests were performed inside the large flume (Figure 2) of the Hydraulic Laboratory, equipped with a wave generation system for maritime physical models at reduced scale. The wave channel is 50m long, 1m wide and 1.3m deep. The flume can work with a maximum water depth of 1m. The sidewalls of the flume are glassed for the central 36m.

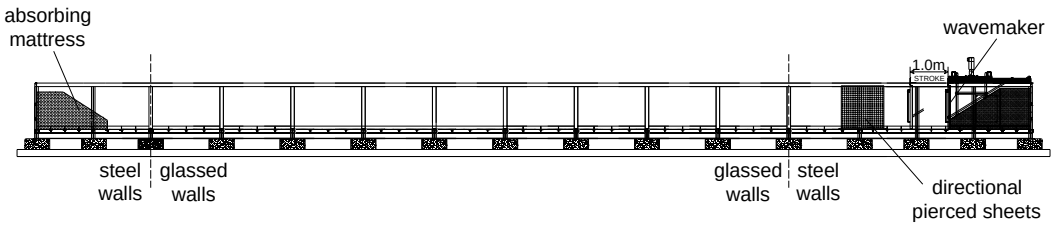

Figure 2: Sketch of the wave flume (cross-section).

The walls of the flume, in which steel vertical rods and large glass windows alternate, allowed to observe the flow from the lateral sides and to video-record it. The waves were forced by a piston-type wavemaker (operating maximum run of 1m). At the opposite end of the flume a wave-absorbing mattress is placed to reduce the wave reflection.

Some hydrodynamic results of 2D experiments on the wave evolution over submerged breakwaters are first presented. In particular, streamwise profiles of water levels collected along the central cross-section of the model as induced by random waves, which represent typical Adriatic sea-storms, are analyzed. The main aim of the first experimental campaign was to understand the influence of different barriers on the morphodynamic evolution of the beach (for more details, see [4]).

In Figure 3 the wave heights due to the wave input OS2 are plotted together with the initial beach profile for two different configurations (B and C). Considering that waves propagate from right to left and that each colored line refers to each phase of the reproduced storm, it is quite clear that an abrupt height decay occurs over the breakwaters (circled in red in the figures). Even if the breakwaters have a quite different distance from the shore in the two configurations, they provide a similar dissipation. Table 1 shows an overview of the transmission coefficients:

$$K_t = \frac{H_t}{H_i} \tag{4}$$

where H_t is the wave height transmitted inshore of the barrier while H_i is the incident wave height and they were chosen as the significant wave heights measured just shoreward and just seaward of the breakwaters, respectively.

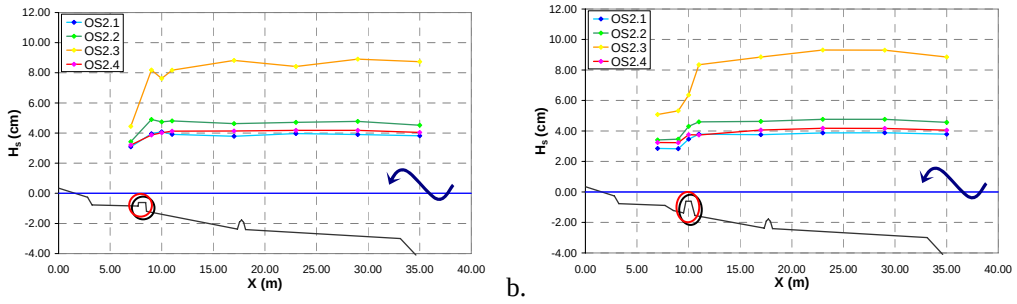

Figure 3: Wave height evolution for configuration B (a.) and C (b.). The black line represents the beach profile, while the colored ones the heights related to the four phases of the sea-storm OS2.

Waves	**OS1.1**	**OS1.2**	**OS1.3**	**OS1.4**	**OS2.1**	**OS2.2**	**OS2.3**	**OS2.4**	**OS3.1**	**OS3.2**	**OS3.3**	**OS3.4**
$\mathbf{K_t}$ - *B*	0.551	0.544	0.558	0.541	0.780	0.698	0.543	0.826	0.454	0.510	0.523	0.581
$\mathbf{K_t}$ - *C*	0.552	0.503	0.526	0.570	0.748	0.753	0.638	0.865	0.446	0.699	0.540	0.600

Table 1: Transmission coefficients K_t for both submerged breakwater configurations.

The values reported on Table 1 refer to the four phases of the three sea-storms tested on both configurations B (lower breakwater close to the shore) and C (higher breakwater further from the shore). A good agreement was found when the experimental coefficients were compared with some theoretical K_t (more details can be found in [4]).

3 EXPERIMENTAL TESTS WITH INNOVATIVE MODELS

The water levels were measured by means of 8 twin-wire resistance gauges. They were located along the flume (see Figure 4), mainly concentrated near the models.

In order to obtain measurements uncorrupted by waves reflected at the end of the flume (the absorbing mattress did not provide complete absorption), models were placed far from the end-mattress (approximately 29m for the former model and 23m for the latter one). This provided quasi-steady measurements for a duration of about 20s. Also a minimal distance was placed between the wavemaker and each model to allow a correct wave formation process.

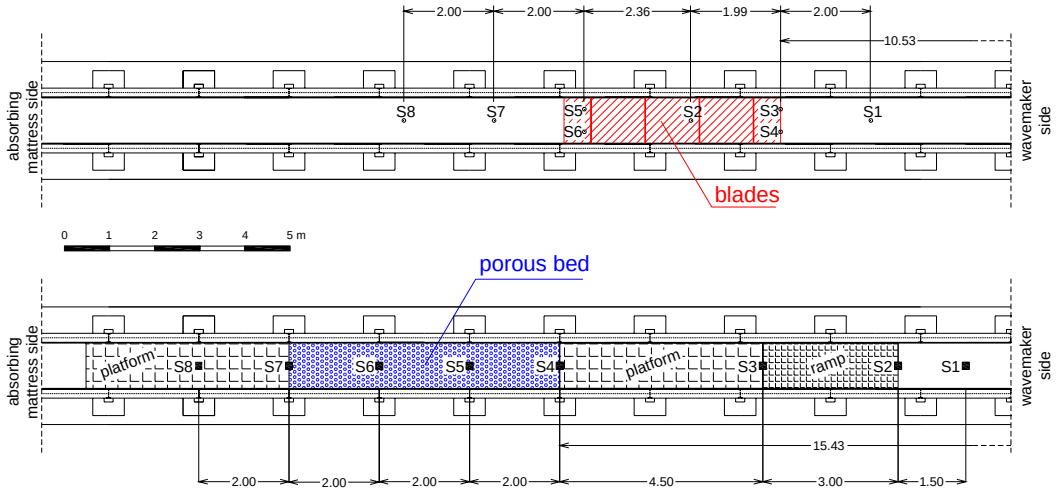

Figure 4: Location of water level gauges (S1-S8) for the two models (plan).

In both tests other instruments were used to know more about the hydrodynamics concerning these innovative dissipative models. The results of such analyses are described in [5], [6], [7], [8] and [9]. Two 3-dimensional ADV (Acoustic Doppler Velocimeters) and one LDA (Laser Doppler Anemometer) were employed to reconstruct the velocity field along the depth, induced by the different configurations. In the case of porous seabed, 7 piezo-resistive pressure transducers were used to evaluate the pressure distribution inside the bed.

Figure 5 illustrates the various seabed configurations used in the experiments.

Figure 5: Seabed configurations with rough structures (a., b.) and porous bed (c.).

3.1 *Tests on vertical and inclined blades*

Focusing on the first set of tests, the physical model, better described in [6] and first proposed

by Nobuoka in [10], is made of a set of rigid structures placed on the bottom of the flume. Each element of the model is made of a steel blade soldered to a horizontal slab to be put down on the bottom of the flume. In order to test different configurations two kinds of blades were used: vertical and inclined at 45° with respect to the flume bottom.

Each model configuration was made of a set of four rows of submerged blades (vertical or inclined) by properly assembling the elements. The tests were performed with four configurations:

i) blades covering the whole flume cross section with vertical blades;

ii) blades covering the whole flume cross section with blade inclination of 45°;

iii) blades covering half of the flume cross section along the right side of the flume, with blade inclination of 45°;

iv) no structures at all.

Whereas the latter two configurations were studied in detail in [7], the former two are analyzed here. Hence, the elements were arranged in four rows of submerged blades, as shown in Figure 6 and described in Table 2, so that the total model length (L_{tot}) was 4.80m and the total width (B) 98cm.

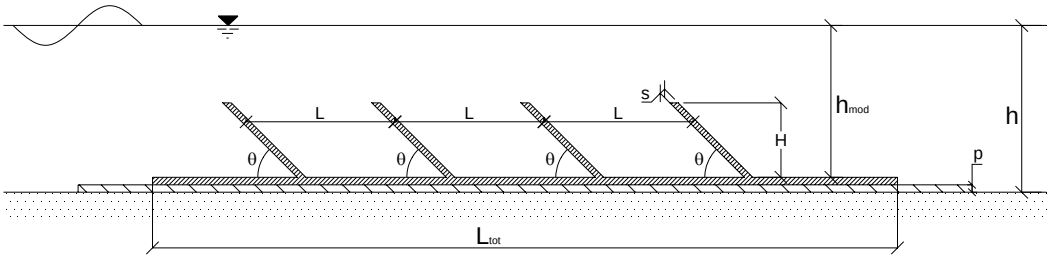

Figure 6: Schematic view of the model (cross-section).

Quantity	**h$_{mod}$** (cm)	**H** (cm)	**s** (cm)	**p** (cm)	**L** (cm)	**a** (cm)	**θ**	**L$_{tot}$** (cm)	**B** (cm)
Size	60	30	1	1.5	120	60	45° - 90°	480	98

Table 2: Geometric characteristics of the models.

The structures were chosen to reproduce the hypothetical field configurations with a reduction provided by a geometric scale of 1:5. Moreover, the time and velocity scales were chosen equal to $1:\sqrt{5}$ in order to satisfy the hydrodynamic Froude similarity. The water depth over the model (h_{mod}) was 60cm and the structure freeboard 30cm, i.e. 3m and 1.5m respectively at prototype scale.

Table 3 shows the characteristics of both regular (wave height H_0 and period T) and spectral JONSWAP waves (H_0=H_s and T=T_p, where H_s is the significant wave height and T_p the peak period) reproduced in the channel, together with the undisturbed water depth (h). More than one run were performed for each wave series (8 regular and 7 spectral) and for each configuration to achieve statistically-significant results.

The regular wave defined as “OR1” was chosen to have the maximum wave height reproducible by means of the wavemaker. Moreover “OR1” and “OR2”, unlike the other regular waves, because of their large steepness reached the model in breaking conditions. Therefore, the energy and height dissipations were mostly due to wave breaking.

The spectral waves OS* were generated by using the JONSWAP spectrum. Even if their names are similar to that of Table 1 (submerged breakwater tests) they are different. A more detailed description of tests performed with such wave inputs is given in [7].

WAVE	**Type**	**h** (cm)	$\mathbf{H_0}$ (cm)	**T** (s)	**WAVE**	**Type**	**h** (cm)	$\mathbf{H_0}$ (cm)	**T** (s)
OR1	regular	60	36	4.025	OS1	spectral	60	20	4.025
OR2	regular	60	30	3.13	OS2	spectral	60	20	3.13
OR3	regular	60	20	2.236	OS3	spectral	60	20	2.236
OR4	regular	60	20	4.025	OS6	spectral	60	25	4.025
OR5	regular	60	20	3.13	OS7	spectral	60	25	3.13
OR6	regular	60	25	4.025	OS8	spectral	60	25	2.236
OR7	regular	60	25	3.13	OS20	spectral	60	30	3.13
OR8	regular	60	25	2.236					

Table 3: Input wave characteristics used for the roughness tests.

3.2 *Tests on permeable beds*

The second set of tests was performed by using a porous bed covering a 6m-long stretch of the horizontal flume bottom. In order to make the waves approach gradually the model some wooden platforms and a 1:15 ramp (ballasted with steel slabs) were used (see Figure 4). The undisturbed water depth over the model was $h=0.30m$.

Three different bottom configurations were considered:

i) a permeable bed;
ii) a rough impermeable layer;
iii) a smooth layer.

Configurations ii) and iii) have been analyzed in detail in the studies [8] and [9]. The permeable bed was made of plastic spheres of 3.6cm in diameter filled with sand. It was composed of six layers which provided a thickness (d) of 18.2cm, so that the relative depth (d/h) was 0.61, the porosity (n) 0.29 and the sphere packing the maximum possible (Figure 5c).

Table 4 shows the input characteristics.

WAVE	**Type**	**h** (cm)	$\mathbf{H_0}$ (cm)	**T** (s)	**WAVE**	**Type**	**h** (cm)	$\mathbf{H_0}$ (cm)	**T** (s)
A	regular	30	3.58	1.00	G	regular	30	15	2.00
B	regular	30	3.58	1.50	H	regular	30	15	2.50
C	regular	30	5	1.50	I	regular	30	20	2.50
D	regular	30	10	1.50	L	spectral	30	10	2.00
E	regular	30	10	2.00	M	spectral	30	10	2.50
F	regular	30	10	2.50	N	spectral	30	15	2.50

Table 4: Input wave characteristics used for the porosity tests.

4 RESULTS AND COMPARISONS

Here the results on wave height dissipation are analyzed. In Figure 7 the wave height streamwise profiles are shown for two of the regular waves used in the tests to demonstrate the

efficiency of the blades (both vertical and inclined). The plot is given in dimensionless form (H/H_0, where H_0 is the input wave height) along the direction of wave propagation (x/L, where $L=3.6m$ is the model length). In all graphs the two lines, representing the mean wave height for blades at 45° (in blue) and 90° (in yellow), are very close one another, suggesting that almost the same dissipation is achieved. Table 5 summarizes the transmission coefficients.

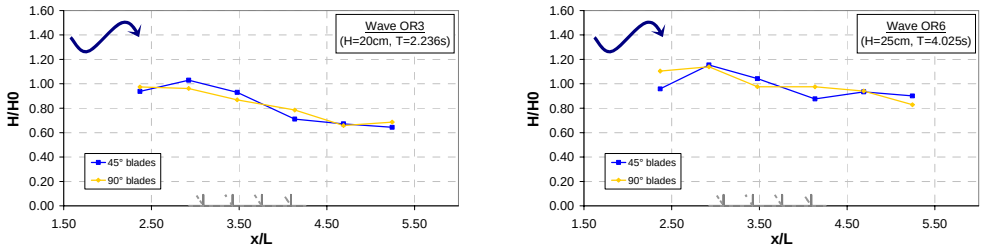

Figure 7: Wave height streamwise profiles for the regular waves OR3 and OR6 over rigid blades, both inclined (blue lines) and vertical (yellow lines).

Waves	**OR1**	**OR2**	**OR3**	**OR4**	**OR5**	**OR6**	**OR7**	**OR8**
$\mathbf{K_t}$ - *45° blades*	0.607	0.607	0.716	0.922	0.599	0.974	0.649	0.741
$\mathbf{K_t}$ - *90° blades*	0.633	0.670	0.675	0.871	0.585	0.852	0.619	0.685

Table 5: Transmission coefficients K_t for both inclined and vertical blade configurations.

Results on the wave dissipation induced by the porous seabed are illustrated in Figure 8, where the model length L is of 6m. The wave height profiles are shown for both permeable bed (blue lines) and rough bed (yellow lines). Such bed configurations induce rather different wave height decays (see also Table 6 which collects the values of K_t induced by the regular waves).

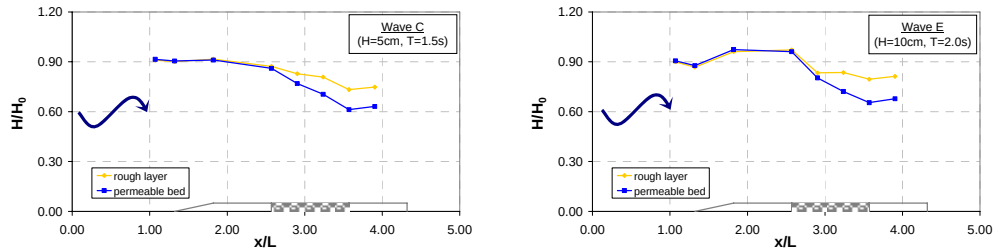

Figure 8: Wave height decay for the regular waves C and E propagating over the permeable bed (blue lines) and the rough bed (yellow lines).

Waves	**C**	**D**	**E**	**F**	**G**	**H**	**I**
$\mathbf{K_t}$ - *rough layer*	0.829	0.807	0.936	0.835	0.933	0.699	0.516
$\mathbf{K_t}$ - *permeable bed*	0.698	0.659	0.772	0.780	0.779	0.679	0.460

Table 6: Transmission coefficients K_t for rough layer and permeable bed configurations.

A simple comparison between the results of Table 5 and Table 6 suggests that the nearbed blades and the permeable seabed provide very similar mean values of the transmission coefficient ($\overline{K_t} \cong 0.70$), i.e. a similar wave height dissipation of about 30%. The rough seabed configuration,

instead, induces a smaller mean decay, less than 20%. Despite the different features of the two tested models, i.e. wave height and period, geometric and temporal scales, wave formation, shoaling phenomenon, comparison of transmission coefficients, only giving the relationship between the wave height upstream and downstream the model, can be regarded as a useful exercise.

5 DISCUSSION AND CONCLUSIONS

Structures made of vertical and inclined blades produce similar wave height decay. Such a decay seems comparable to that induced by geometrically-equivalent submerged breakwaters with similar submergence and cross-section, highlighting the effectiveness in reducing the wave heights produced by the nearbed macro-roughness due to the blades.

The wave dissipation provided by a porous seabed depends on the wave characteristics, such as the wave height and the wavelength, but it is also influenced by the bed geometric features, such as thickness and length.

The results reported here confirm that both the porous medium and the nearbed rigid blades induce a wave height reduction of 20-30%, hence the terms ε_f and ε_p which appear in (1) can give a contribution comparable to that of ε_b.

A better characterization of the working of the models at hand requires a sounder explanation of the wave height decay in terms of the total energy budget. Hence, a much better description of the internal flow kinematics is needed. To this purpose we inspected the flow by means of a non-intrusive approach which makes use of optical velocimetry methods to derive, directly from available video images, the extended hydrodynamic fields characterizing the internal kinematics of the flow at hand.

The next figure shows an example of the flow circulation on a longitudinal vertical section as derived from trajectories obtained by means of the FT-PTV (Feature Tracking - Particle Tracking Velocimetry) technique.

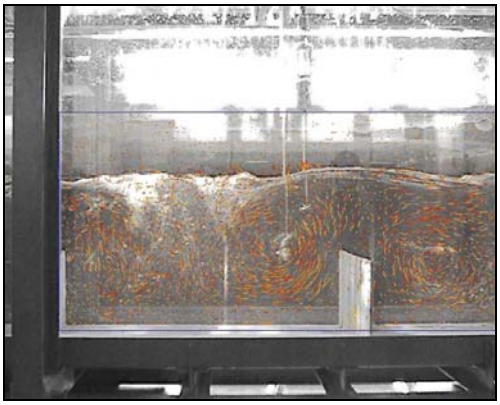

Figure 9: Description of the motion field by means of the FT-PTV.

For the vertical and inclined blades some analyses reveal the presence of large-scale vortices with horizontal axes (macrovortices) which are believed to be responsible for much of the wave energy draining in favour of vortical features of various sizes (from the integral scale to the dissipative one). It is clear that, because of the flow unsteadiness, each analyzed cell between two nearby blades can contain two counter-rotating vortices instead of the single vortex which would

characterize a steady flow.

The energy dissipation which characterizes the flow seems to have a different contribution from the various turbulent and vorticity patterns which are specific of each seabed configuration. As above mentioned, in the case of the nearbed blades, macrovortices form inside the cells and cover the whole water column, also influencing the water surface. Instead, in the other case, the turbulence generated on the permeable seabed stays confined within the bottom boundary layer. The presence of the permeable bed reduces the average horizontal and vertical velocities of the incident wave, with a consequent kinetic energy decay of the wave itself. The main dissipation occurs inside the porous bed because of the drag and inertia forces characterizing the interaction between the oscillatory flow and the spheres.

Finally a complete comparison between the models is difficult, since they are similar in dimensions and efficiency but a real economic estimation about their construction and maintenance may be hard to do.

References

[1] Stive, M.J.F., "Energy dissipation in waves breaking on gentle slopes," *Coastal Engineering*, **8**, Issue 2, 99-127 (1984).

[2] Piattella, A., Mancinelli, A., "Idrodinamica costiera generata da "strutture dissipative"," *Atti 30° Convegno Nazionale di Idraulica e Costruzioni Idrauliche*, Roma, Italy, September 10-15, 2006, CD-ROM (2006).

[3] Brocchini, M., Kennedy, A., Soldini, L., Mancinelli, A., "Topographically controlled, breaking-wave-induced macrovortices. Part 1. Widely separated breakwaters," *Journal of Fluid Mechanics,* **507**, 289-307 (2004).

[4] Lorenzoni, C., Mancinelli, A., Postacchini, M., Soldini, L., "Experimental tests on a sandy beach model protected by low-crested structures," *Proc. 4th International Short Conference on Applied Coastal Research*, Barcelona, Spain, June 14-17, 2009 (in print).

[5] Brocchini, M., Lorenzoni, C., Mancinelli, A., Soldini, L., "Un'analisi preliminare del funzionamento di strutture di difesa costiera dissipanti per macroscabrezza," *Atti del 18° Congresso dell'Associazione Italiana di Meccanica Teorica e Applicata,* Brescia, Italy, September 11-14, 2007, CD-ROM (2007).

[6] Lorenzoni, C., Soldini, L., Brocchini, M., Mancinelli, A., Postacchini, M., Seta, E., Corvaro, S., "On the working of defence coastal structures dissipating by macro-roughness," *Journal of Waterway, Port, Coastal, and Ocean Engineering* (in print).

[7] Lorenzoni, C., Brocchini, M., Mancinelli, A., Soldini, L., Seta, E., Postacchini, M., "An experimental analysis of the hydrodynamics of submerged structures dissipating by macro-roughness," *Proc. 2nd International Conference on Application of Physical Modelling to Port and Coastal Protection*, Bari, Italy, July 2-5, 2008 (in print).

[8] Corvaro, S., Mancinelli, A., Lorenzoni, C., Seta, E., Postacchini, M., "Study of the wave damping due to a porous bed," *Proc. 2nd International Conference on Application of Physical Modelling to Port and Coastal Protection*, Bari, Italy, July 2-5, 2008 (in print).

[9] Corvaro, S., Lorenzoni, C., Mancinelli, A., Postacchini, M., Seta, E., "Prove sperimentali in canale per onde di mare su fondo permeabile," *Atti 31° Convegno Nazionale di Idraulica e Costruzioni Idrauliche*, Perugia, Italy, September 9-12, 2008, CD-ROM (2008).

[10] Nobuoka, H., Irie, I., Kato, H. and Mimura, N., "Regulation of nearshore circulation by submerged breakwater for shore protection," *Proc. 25th International Conference on Coastal Engineering,* Orlando, FL, U.S.A., 2394-2403 (1996).